Volume 13
Number 47
21 December 2025
Pages 15137–15438

Journal of Materials Chemistry B

Materials for biology and medicine

rsc.li/materials-b

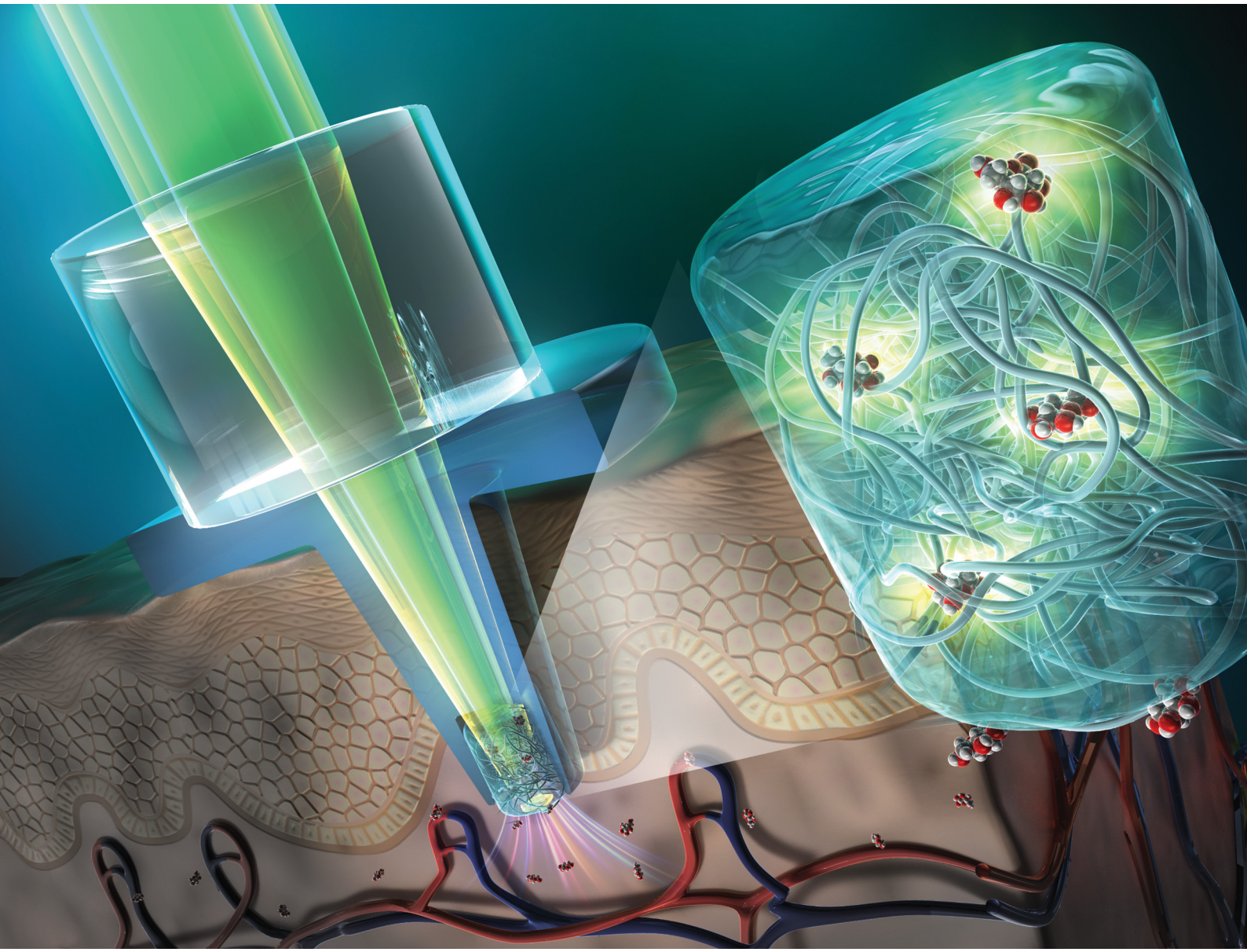

ISSN 2050-750X

ROYAL SOCIETY OF CHEMISTRY

PAPER

Hiroaki Takehara *et al.*
Development of an optical microneedle device embedding sub-nanoliter volumes of boronic acid-based fluorescent hydrogel

Journal of Materials Chemistry B

ROYAL SOCIETY OF CHEMISTRY

PAPER

View Article Online
View Journal | View Issue

Cite this: J. Mater. Chem. B, 2025, 13, 15273

Development of an optical microneedle device embedding sub-nanoliter volumes of boronic acid-based fluorescent hydrogel

Masahiro Fukuhara,[a] Hiroaki Takehara, *[ab] Kevin Barthelmes,[c] Benjamin Kersch-Hunt,[d] Jordan E. Gardiner,[def] Yukihiro Kanda,[ab] Akira Matsumoto,[ac] Tony D. James[dg] and Takanori Ichiki[ab]

Received 20th February 2025,
Accepted 24th October 2025

DOI: 10.1039/d5tb00385g

rsc.li/materials-b

Although the diagnostic utility of interstitial fluid (ISF) has been extensively explored, collecting and sensing ISF remains challenging. Microneedle devices offer a promising approach as a minimally invasive method to obtain ISF in a small volume or to sense biomolecules in the ISF within the body. However, conventional enzymatic measurements consume target molecules, compromising sensing reliability, especially in a small volume. To overcome the above issue, we developed fluorescence-based optical microneedles for non-consumptive molecular sensing within tiny ISF samples. The optical microneedle was functionalized with a small-volume fluorescent hydrogel block at its tip. The hydrogel block measured 100 μm in diameter and 100 μm in length, with a total volume of 0.79 nL. The microneedle made of amorphous poly-L-lactide (PLLA) had a high-aspect ratio shape (500 μm in base diameter, 200 μm in top diameter, and 2 mm in length), reaching the ISF near the vascular plexus in the reticular layer. In addition, the fluorescent hydrogel was functionalized with boronic acid, which reversibly binds to D-glucose. As proof of our technology, we conducted D-glucose sensing using an optical microneedle. The average value of measurement errors from actual D-glucose concentrations was calculated to be 5.6% in the range of 6.1 to 37.5 mM. Therefore, it was confirmed that the microneedle device is useful for ISF measurements.

1. Introduction

Wearable biosensors have emerged as a promising technology for monitoring human physiological states, particularly for their role in advancing healthcare and enabling the early diagnosis of diseases.[1,2] Bioabsorbable polymers are promising materials for biosensing devices. Recently, microfabrication technologies have been developed to minimize the invasiveness of such devices.[3,4] In this context, microneedles made of bioabsorbable polymers, originally developed for minimally invasive transdermal drug delivery,[5–12] have attracted interest for diagnostic applications because of their molecular sensing capabilities.[13–17]

The interstitial fluid (ISF) contains numerous biomolecules that are useful for diagnosis. The most notable diagnostic application of ISF is in the monitoring of D-glucose levels to manage diabetes. Several devices for continuous glucose monitoring have already been adopted in clinical practice.[18–20] Because of their success in monitoring D-glucose *via* ISF, the utility of ISF for diagnosis has been gaining increasing attention. However, collecting diagnostically relevant ISF is more challenging than collecting blood because extracting dermal ISF disrupts the delicate pressure balance between the inside and outside of blood vessels.[21] Therefore, methods for sampling ISF with extraction of small volumes (sub-nanoliters) of liquid or for *in situ* sensing of ISF using miniaturized sensors are necessary.

First, one of the critical technical barriers in molecular measurement within such small volumes lies in the use of conventional approaches using enzymatic reactions (*e.g.* glucose oxidase-based assays). These methods inevitably consume the target molecules during detection, thereby perturbing their original concentration and compromising the reliability of the measurement especially for small volume samples. To address this limitation, fluorescence-based techniques, which do not consume the analyte during detection, offer a promising solution. The present study provides a technological advancement by realizing

[a] Department of Materials Engineering, School of Engineering, The University of Tokyo, Tokyo, 113-8656, Japan
[b] Innovation Center of NanoMedicine, Institute of Industry Promotion, Kawasaki, Kanagawa, 218-0821, Japan
[c] Laboratory for Biomaterials and Bioengineering, Institute of Science Tokyo, Tokyo, 101-0062, Japan
[d] Department of Chemistry, University of Bath, Bath, BA2 7AY, UK
[e] Lifecare Chemistry, Bath, BA2 4BL, UK
[f] Lifecare Chemistry Laboratory, Science Creates, Bristol, BS2 0XJ, UK
[g] School of Chemistry and Chemical Engineering, Henan Normal University, Xinxiang, 453007, China

glucose sensing for small volumes of sub-nano-litter ranges at the microneedle tip through a fluorescence-based method.

Second, for molecular sampling and sensing in the body using microneedles, it is preferable for the microneedles to reach the ISF near the vascular plexus in the reticular layer. Previously, we developed poly-L-lactide (PLLA) microneedles with a length of 2 mm that reach the reticular layer.[22] These PLLA microneedles were fabricated using vacuum-assisted molding processes, which could insert into porcine skin tissues.[23] Moreover, to develop microneedles for diagnosis, we have reported a fabrication technique for functionalizing the tips of PLLA microneedles using hydrogel photopolymerization, enabling them to extract small volumes of liquid or sense biological molecules within the body.[24]

In this paper, D-glucose sensing using PLLA microneedles was conducted to prove our fluorescence-based technology. Our device uniquely achieves glucose detection in sub-nanoliter volumes at the needle tip, thereby enabling highly localized and short-term measurements in the body. Optical microneedles functionalized with a fluorescent hydrogel containing boronic acid, which reversibly binds to D-glucose, were fabricated, and their responsiveness to varying D-glucose concentrations in solution was evaluated. These experiments demonstrated the potential of optical microneedles as a platform for sensing various biomolecules.

2. Experimental

2.1 Concept of *in situ* fluorescence sensing

Fig. 1a and b depict schematics of *in situ* fluorescence sensing using a microneedle with a high-aspect ratio. The microneedle was designed to have a length of 2 mm, allowing it to reach the ISF near the blood vessels. Optically transparent PLLA microneedles were used as optical waveguides. The microneedle tip was functionalized with a hydrogel block and fixed to a fluorescent probe, as shown in Fig. 1b. The hydrogel block facilitates the sampling of ISF with sub-nanoliter volumes of liquids and serves as a reaction space for sensing biological molecules in the body.

2.2 PLLA microneedle with gradient index lens

PLLA is one of the most promising thermoplastics and is known for its high strength and modulus. It holds significant potential for biomedical applications as a bioabsorbable and biocompatible semicrystalline polymer.[25–27] In this study, the device was designed to integrate the PLLA microneedle with a gradient-index (GRIN) lens, enabling precise light focusing on the position of the microneedle tip. The PLLA microneedle with a high aspect ratio (500 μm in base diameter, 200 μm in top diameter, and 2 mm in length) was produced through vacuum-assisted molding processes adapted from the literature,[22] as shown in Fig. 2. A phosphor bronze master mold of a microneedle with a pocket structure (100 μm in diameter and 100 μm in depth) was manufactured using an ultra-precision mechanical processing machine (ROBONANO α-0iB, FANUC Corp., Japan). Poly-dimethylsiloxane (PDMS) (BASE : CAT = 10 : 1.5) was cured (120 °C, 2 h) on the master mold. The cured PDMS mold was then removed from the master mold. Then, the PDMS mold and PLLA pellets were degassed at 0.1 hPa for 10 h. PLLA pellets were melted at 0.1 hPa and 195 °C. After quenching for 5 min on a thermoelectric cooler set to 10 °C to rapidly pass through its crystallization temperature (120–130 °C), the PLLA microneedle was demolded from the PDMS mold.

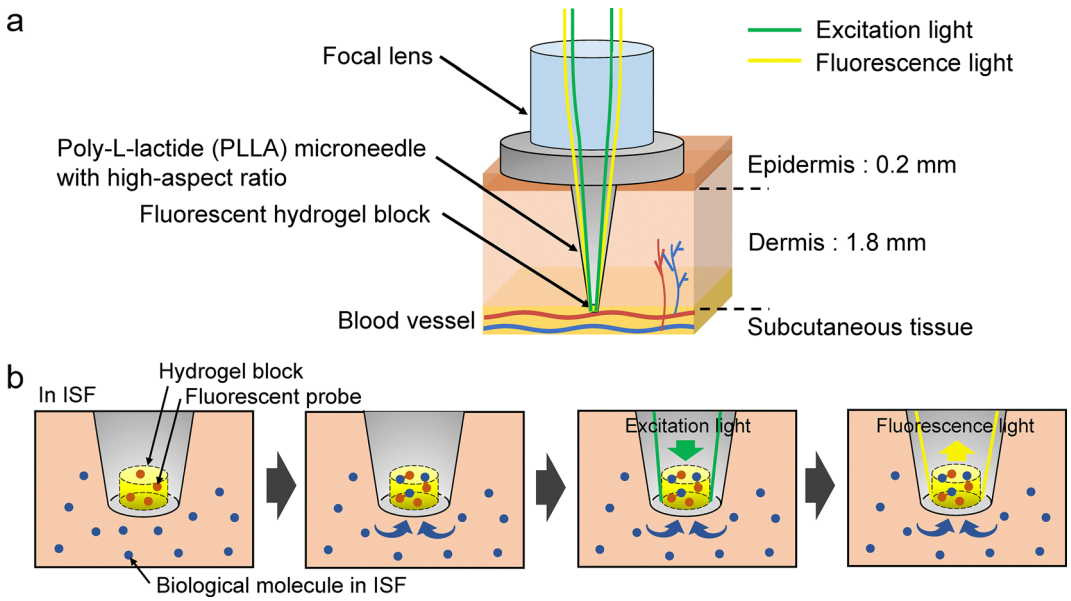

Fig. 1 Schematic illustration of *in vivo* fluorescence sensing using a microneedle. (a) PLLA microneedle with high-aspect ratio (500 μm in base diameter, 200 μm in top diameter, and 2000 μm in length) with a hydrogel block (100 μm in diameter and 100 μm in length, total volume: 0.79 nL) at the needle tip. (b) Schematic illustration of functionalized microneedle tip. The hydrogel block enables the extraction of biological molecules by diffusion and serves as a reaction space for *in situ* molecular sensing.

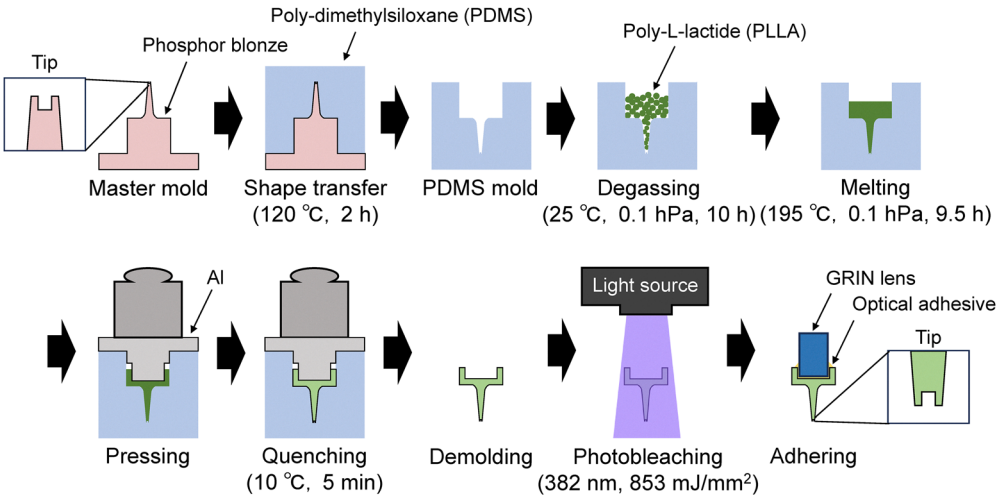

Fig. 2 Fabrication process of PLLA microneedle with the GRIN lens using vacuum-assisted molding process. Initially, PDMS was cured (120 °C, 2 h) on the master mold and removed from it. Subsequently, the PDMS mold and PLLA pellets were degassed at 0.1 hPa for 10 h. PLLA pellets were melted at 0.1 hPa and 195 °C for 9.5 hPa. After quenching for 5 min with an aluminum lid, the PLLA microneedle was demolded from the PDMS mold and photobleached for 5 h. Finally, the fabricated PLLA microneedle and the GRIN lens were integrated using optical adhesives.

Subsequently, UV light (382 nm, 853 mJ mm^{-2}) was irradiated onto the PLLA microneedle to induce photobleaching. This process was performed to eliminate the influence of PLLA autofluorescence during sensing using the device. Finally, the fabricated PLLA microneedle and the GRIN lens were integrated using refractive-index-matching adhesives (Thorlabs, NOA65). A specially designed GRIN lens (NA: 0.51, 1.8 mm diameter and 2.4 mm length) was fabricated by Go; Foton Japan R&D Systems.

2.3 Crystallinity and optical transmittance measurements

To clarify the optical properties of PLLA, the crystallinity and optical transmittance of PLLA sheets (20 mm in width, 20 mm in height, and 0.1 mm in thickness) were measured. Crystallinity was measured using an X-ray diffractometer (Rigaku, SmartLab). X-ray diffraction measurements were performed by irradiating the PLLA sheet samples fixed in a slit with a 1000 mm-wide parallel X-ray beam. The measurement range was 5.0° to 50°, with a step width of 0.050° and a scan speed of 20° min^{-1}, recording the diffraction intensity in counts per second (cps). The optical transparency was evaluated using a spectrophotometer (JASCO, V670). The scan speed was set to 1000 nm min^{-1}, and the measurement range covered wavelengths from 3200 to 190 nm to record the transmittance (%*T*).

2.4 Synthesis of glucose responsive fluorescent hydrogel

Photopolymerization provides spatial control during the formation of three-dimensional hydrogels. In this study, UV light was focused on microneedle tips for photopolymerization during functionalization. Hydrogels were formed by copolymerizing acrylamide and *N*,*N*′-methylenebis(acrylamide) *via* free-radical polymerization. The photoinitiator 2-hydroxy-4′-(2-hydroxyethoxy)-2-methylpropiophenone (Irgacure® 2959) was sourced from Sigma-Aldrich. Acrylamide was purchased from Bio-Rad (Hercules, CA). *N*,*N*-methylenebis(acrylamide) was obtained from FUJIFILM Wako Pure Chemical Corporation.

A boronic acid-based anthracene monomer was prepared to functionalize the hydrogel for D-glucose sensing as a proof of technology.[28] The modification of hydrogels to contain boronic-acid binding motifs enables the optical properties of the hydrogel to be reversibly modulated through exposure to saccharide-containing stimuli. The solution for D-glucose responsive fluorescent hydrogels (Glu–Flu hydrogel) was prepared by dissolving 2.42 wt% Irgacure® 2959, 19.4 wt% acrylamide, 1.45 wt% *N*,*N*′-methylenebis (acrylamide) and 0.03 wt% boronic acid-based anthracene monomer in methanol (Scheme S1).

2.5 Functionalization of microneedle tip

Using the fabricated PLLA microneedle with the pocket structure, the hydrogel embedding process was performed following a previous report.[24] Fig. 3 depicts the schematic illustration of the hydrogel embedding process at the needle tip using photopolymerization. First, the PLLA microneedle was immersed in the monomer solution, and its tip was attached to the surface of the elastic PDMS sheet. The irradiated light was introduced into the PLLA microneedle from the base using a GRIN lens. The microneedle tip was irradiated (382 nm, 0.83 W mm^{-2}). Subsequently, the microneedle was removed from the monomer solution and immersed in water for 20 min to replace methanol with water.

2.6 Numerical analysis of D-glucose diffusion

Computational simulation of mass transportation was conducted using a finite element method (FEM) simulator (COMSOL Multiphysics 6.3). Diffusion coefficient of D-glucose was set as 220 μm cm^{-2}. The initial concentrations of D-glucose in the hydrogel at the microneedle tip and the surrounding ISF were set to 0.0 and 40.0 mM, respectively. Calculations were performed over the range of 0 to 200 s.

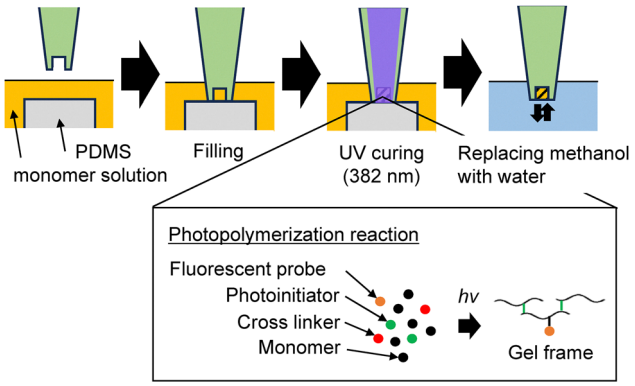

Fig. 3 Embedding process of fluorescent hydrogel at the microneedle tip using photopolymerization method. Initially, the tip of the PLLA microneedle was immersed in the monomer solution, filling the pocket structure. Subsequently, irradiation light (382 nm) was delivered through the inside of the PLLA microneedle, initiating the photopolymerization reaction at the microneedle tip. Finally, methanol was replaced with water.

2.7 Fluorescence measurements

The boronic acid group of the Glu–Flu hydrogel reversibly binds to D-glucose in the solution. Glucose sensing can be performed by measuring changes in the fluorescence intensity of the Glu–Flu hydrogel in response to the D-glucose concentration. The D-glucose responsiveness of the Glu–Flu hydrogels was normalized to the fluorescence intensity ratio relative to the intensity at a D-glucose concentration of 0 mM.

First, bulk samples (8 mm in diameter and 0.5 mm in thickness) with boronic acid-based anthracene monomer concentration of 0.03 wt% were fabricated. Subsequently, the fabricated hydrogels were fixed in glass cells and immersed in D-glucose solutions of various concentrations. After sufficient immersion, fluorescence spectra were obtained in the range of 395–460 nm at an excitation wavelength of 382 nm using a spectrofluorometer (Shimadzu, RF-6000). The fluorescence acquisition interval was set to 1.0 nm, and the scan speed was set to 2000 nm min^{-1}. For the fluorescence titrations, the spectrometer parameters were fixed as: slit, 1.5 nm/5.0 nm, scan speed: 2000 nm min^{-1}.

2.8 Optical design for glucose sensing

Fig. 4 shows a schematic of the optical system used for D-glucose sensing using the microneedles. The microneedle tip, functionalized with the Glu–Flu hydrogel, was immersed in D-glucose solutions of different concentrations. The excitation laser light from a laser diode (NICHIA, NDU7212E) passed through a bandpass filter (CWL: 375 nm, FWHM: 28 nm) and was reflected by a dichroic mirror (Refl. (>95%): 350–407 nm, *Trans.* (>95%): 415–650 nm). It is then focused onto the microneedle tip using a GRIN lens. Subsequently, the fluorescence emitted from the Glu–Flu hydrogel passed through the GRIN lens, dichroic mirror, bandpass filter (CWL: 431 nm, FWHM: 28 nm), and convex lens (focal length: 25 mm) and was detected by an avalanche photodiode (Thorlabs, APD410A2/M, multiplication factor: 50). The dichroic mirror and bandpass filter were sourced from Chroma Technology Corporation. Each measurement result was obtained using a digital multimeter while the laser was irradiated for 30 s.

3. Results and discussion

3.1 Fabrication of PLLA microneedle with GRIN lens

Fig. 5a and b show bright-field images of the fabricated microneedle-type device with a GRIN lens. The high-aspect ratio shape of the PLLA microneedle, with dimensions of 500 μm in base diameter and 2 mm in length, was observed in Fig. 5a. The distance from the tip surface of the microneedle to the end surface of the GRIN lens was measured to be 5.5 mm,

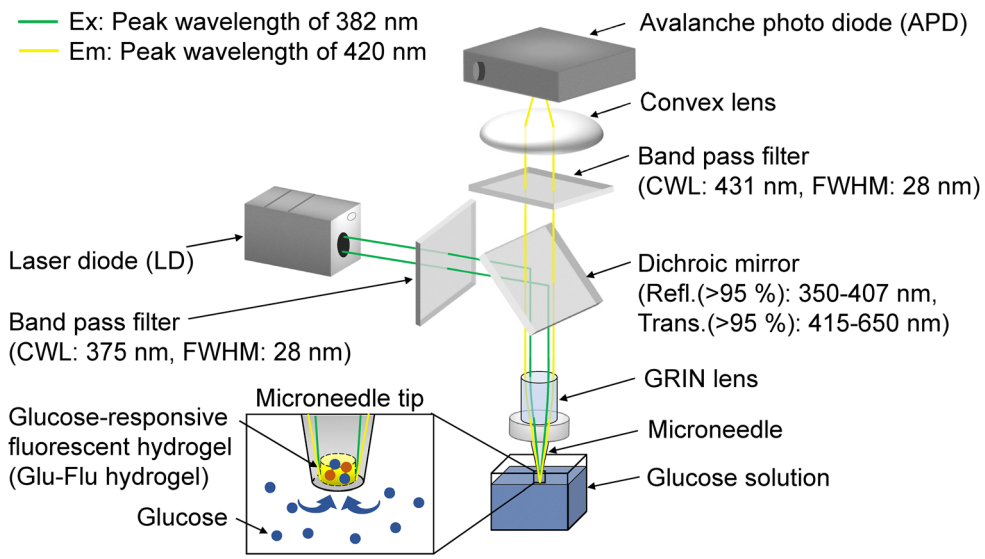

Fig. 4 Schematic diagram of the optical system for D-glucose sensing. The excitation light was focused onto the microneedle tip functionalized with Glu–Flu hydrogel. The microneedle tip was immersed into the D-glucose solution. The fluorescence light from Glu–Flu hydrogel was detected by APD.

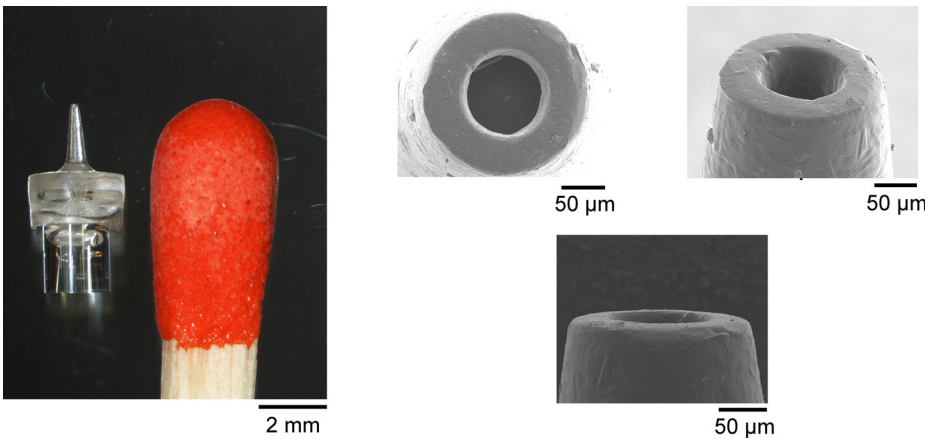

Fig. 5 Fabricated PLLA microneedle-type device. (a) Photograph showing the microneedle-type device. The length of the device was equivalent to the tip of a matchstick. (b–d) SEM image of the PLLA microneedle tip (200 μm in top diameter) featuring the pocket structure for hydrogel embedding (100 μm in diameter and 100 μm in depth) viewed from the top (b), at an angle (c), and from the side (d).

and the width of the device was measured to be 2.6 mm. Fig. 5c–f display SEM images of the PLLA microneedle at low and high magnifications, respectively. Additionally, the diameter of the pocket structure at the needle tip was measured to be 97 ± 7 μm, confirming the precision of our molding process.

3.2 Transparency of PLLA

To utilize PLLA microneedles as optical waveguides, they must be optically transparent. In general, the crystallization of polymer materials affects their optical transparency; therefore, it is necessary to control the crystallization of the material during thermal processing.[29,30] Fig. 6a shows the relationship between the crystallization time and crystallinity of the PLLA sheets. A fitting curve based on the Kolmogorov–Johnson–Mehl–Avrami equation was obtained (see SI).[31–33] Additionally, Fig. 6b shows the relationship between the crystallinity and optical transmittance at 382 and 420 nm in the PLLA sheets. The optical transmittance decreases exponentially with increasing crystallinity. Therefore, it is desirable to fabricate PLLA in a completely amorphous state so that microneedles can function as optical waveguides.

3.3 Embedding of hydrogel at microneedle tip

Fig. 7a shows the relationship between the embedded Glu–Flu hydrogel's thickness and the UV light's energy (382 nm) irradiating the microneedle tip. The thickness increased linearly until the irradiation energy reached 315 mJ, and the Glu–Flu hydrogel fully filled the pocket structure. Fig. 7b and c depict the optical microneedle with the Glu–Flu hydrogel embedded at the tip. The volume of the pocket at the tip designed for embedding a hydrogel block was 0.79 nL (100 μm in diameter and 100 μm in depth). The boronic-acid-based anthracene monomer bound to the polyacrylamide frame emitted fluorescence with a peak wavelength of 420 nm when excited at 382 nm. Fluorescence emitted by the hydrogel embedded at the microneedle tip was observed through fluorescence images (E_x: 382 ± 7 nm, E_m: 431 ± 14 nm) as shown in Fig. 7c. Through the combination of a focus lens (GRIN lens) and a waveguide (optically transparent PLLA microneedle), the irradiation area was localized at the microneedle tip.

3.4 Glucose diffusion at the microneedle tip

To precisely numerically estimate the reading time fort sensing glucose using optical microneedles, FEM based on mass

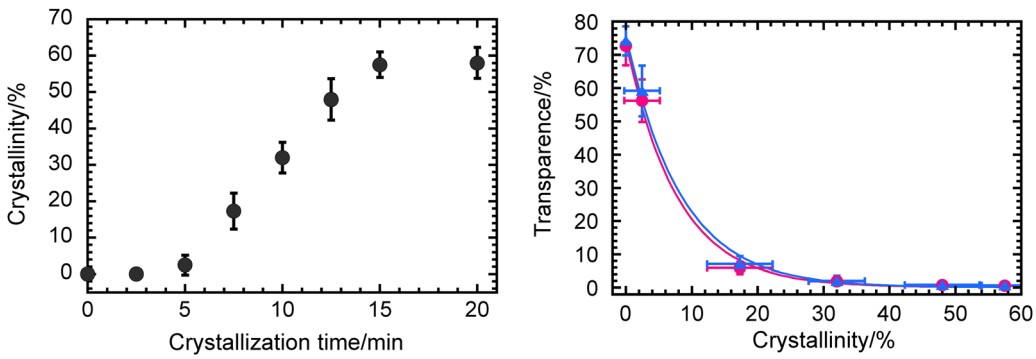

Fig. 6 The effect of PLLA crystallinity on its optical properties. (a) Relationship between crystallization time and crystallinity in PLLA sheets (20 mm in width, 20 mm in height and 0.1 mm in thickness). (b) Relationship between crystallinity and optical transmittance at 382 nm and 420 nm in PLLA sheets. Data are means ± SD (n = 2–3).

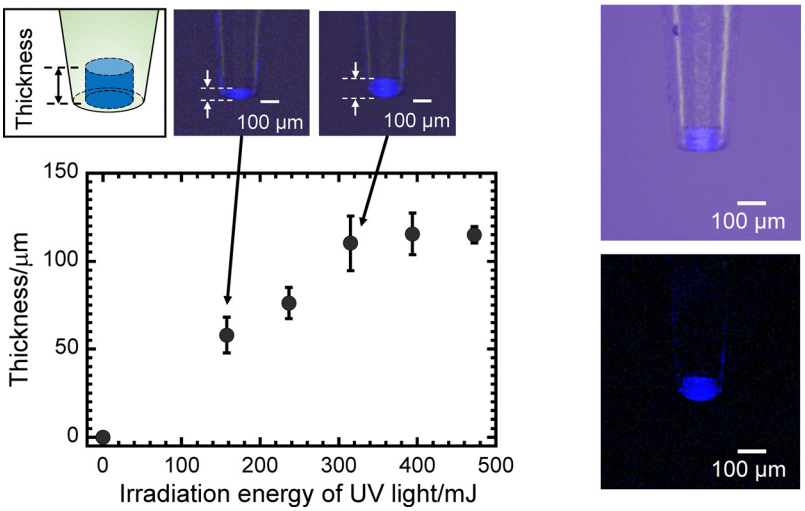

Fig. 7 Glu–Flu hydrogel embedded at the microneedle tip. (a) Relationship between the thickness of the embedded Glu–Flu hydrogel and the energy of UV light irradiated at the microneedle tip for photopolymerization of the Glu–Flu hydrogel during the embedding process. Error bars represent measurement errors. (b) Overlay image of bright-field image and fluorescence image and (c) fluorescence image of functionalized microneedle tip with Glu–Flu hydrogel. (E_x: 382 ± 7 nm, E_m: 431 ± 14 nm).

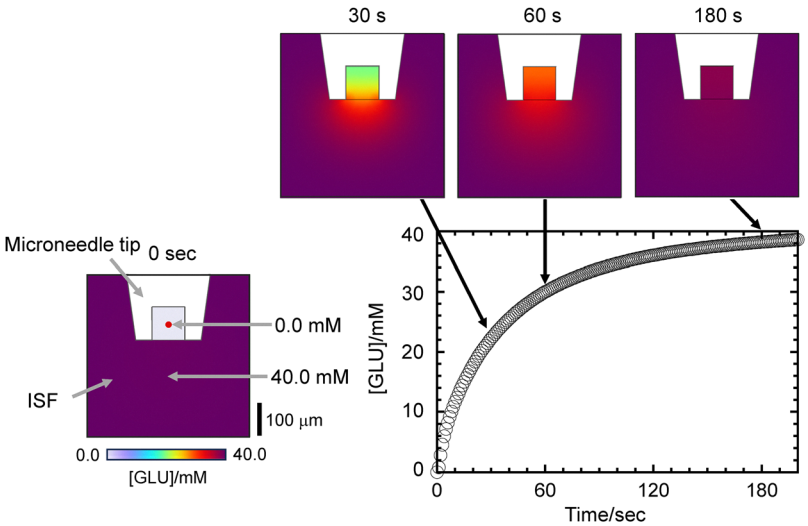

Fig. 8 Numerical analysis of D-glucose diffusion at the microneedle tip. Time sequential change of the concentration of D-glucose in the hydrogel at the microneedle tip and the surrounding ISF was calculated. The plots show the concentration of D-glucose at the red point in the hydrogel.

transformation analysis was performed. Fig. 8 shows the time sequential change of the concentration in the hydrogel at the microneedle tip and the surrounding ISF. The fluorescence response at the microneedle tip became detectable at 180 s with over 95% accuracy of the concentration in ISF and responded to localized concentration in ISF within 200 μm in distance. The rapid and localized measurement arises from two aspects: (1) the sensor reads D-glucose directly at the tip so no bulk extraction is required, and (2) the reading time is dominated by D-glucose diffusion into the small volume sensing region (sub-nL).

3.5 Glucose responsiveness of Glu–Flu hydrogel

Fig. 9 shows the relationship between the fluorescence intensity ratio and the D-glucose concentration. A fitting curve based on a theoretical equation was obtained from the measurement results (see SI). The coefficient of determination (R^2) of the measured values against the fitting curve was 0.93. The obtained fitting curve was used as the calibration curve for D-glucose sensing using an optical system integrated with a microneedle-type device embedded with a Glu–Flu hydrogel at the microneedle tip.

3.6 Glucose sensing using microneedle-type optical system

Fig. 10 shows the results of the fluorescence sensing of D-glucose concentration using a microneedle-type optical system. The fluorescence from the Glu–Flu hydrogel at the microneedle tip was measured after immersion in solutions with D-glucose concentrations of 0, 6.1, 12.9, 21.5, and 37.5 mM. Table 1 shows the calibration values for the D-glucose concentration

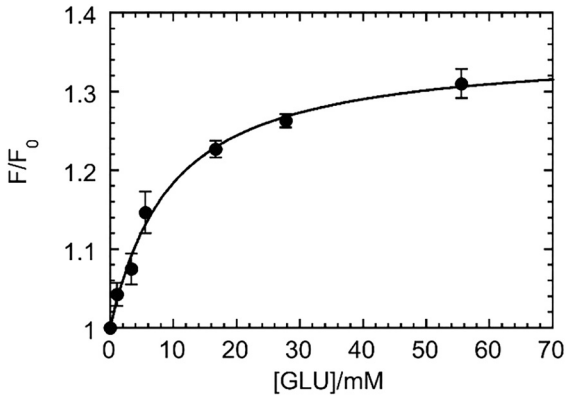

Fig. 9 Relationship between fluorescence intensity ratios (F/F_0) of D-glucose-responsive fluorescent bulk hydrogel at 417–445 nm and D-glucose concentration in pH 8.50 buffer solution. F represents an integrated fluorescence intensity from 417 nm to 445 nm. F_0 represents the value of F under D-glucose concentration of 0 mM. The calibration curve was obtained by fitting the measured values based on a theoretical equation (sample size: n = 3, coefficient of determination: R^2 = 0.93).

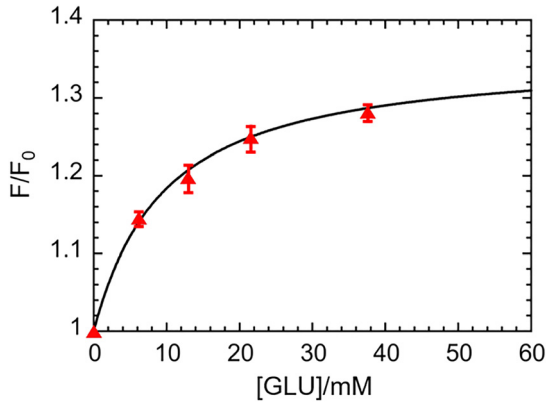

Fig. 10 Fluorescence intensity ratios (F/F_0) at 417–445 nm obtained from the fluorescence sensing using the optical system integrated with microneedle-type device under D-glucose concentrations of 0, 6.1, 12.9, 21.5 and 37.5 mM in pH 8.50 buffer solution. Error bars represent measurement errors. The curve represents the calibration curve obtained from the experiments with D-glucose-responsive fluorescent bulk hydrogel.

Table 1 The calibration values of D-glucose concentration measured using the microneedle-type optical system and their errors relative to the actual D-glucose concentrations

[GLU]/mM	F/F_0	Calibrated value/mM	Error of calibrated value/%
6.1	1.15	6.5	4.9
12.9	1.20	11.7	9.6
21.5	1.25	21.5	0.0
37.5	1.28	34.6	7.9

calculated using the calibration curve, the measured fluorescence intensity ratios, and their errors relative to the actual D-glucose concentrations. The errors of calibrated value were calculated to be 4.9% at 6.1 mM, 9.6% at 12.9 mM, 0.0% at 21.5 mM, and 7.9% at 37.5 mM. For reference, a blood glucose meter for self-testing must have at least 95% of its measurements within a 15% margin of error for D-glucose concentrations of 5.6 mM or higher.[34]

In this study, D-glucose measurement was feasible only under weakly alkaline conditions (pH 8.5), consistent with a previous report.[28] However, the optical probe in the hydrogel can be replaced with different optical probes. Therefore, following the concept of fluorescence sensing using an optical microneedle, the required sensitivity and selectivity for measuring the target biomolecules can be achieved by switching to other optical probes.

4. Conclusions

In this study, we evaluated the D-glucose responsiveness of optical PLLA microneedles embedded in fluorescent hydrogels at their tips. Optical microneedles were fabricated using a vacuum-assisted molding and integrated with a focal lens (GRIN lens). Glu–Flu hydrogels were embedded in microneedle tips with a pocket structure using a photopolymerization process. A calibration curve based on a theoretical equation was obtained to evaluate the D-glucose responsiveness of the bulk Glu–Flu hydrogel samples. As proof of our technology, the D-glucose responsiveness of the optical microneedles to varying D-glucose concentrations in solution was evaluated. Errors of calibrated values from actual D-glucose concentrations were calculated to be 4.9% at 6.1 mM, 9.6% at 12.9 mM, 0.0% at 21.5 mM, and 7.9% at 37.5 mM. An optical microneedle device integrated with a mono-boronic acid-based fluorescent hydrogel was developed, and the evaluated values showed potential for use in D-glucose sensing in ISF.

Author contributions

MF: writing – original draft, methodology, investigation, formal analysis, data curation. HT: writing – review & editing, supervision, investigation, formal analysis, data curation, funding acquisition, conceptualization. KB: writing – original draft, methodology, materials synthesis and characterization, data curation. BKH: writing – review & editing, methodology, investigation, formal analysis, data curation. JEG: supervision, funding. YK: writing – review & editing, methodology, investigation. AM: writing – review & editing, supervision, funding acquisition, conceptualization. TDJ: writing – review & editing, supervision, funding. TI: supervision, funding acquisition, conceptualization.

Conflicts of interest

The authors declare that they have no known competing financial interests or personal relationships that could have appeared to influence the work reported in this paper.

Data availability

All data generated or analysed during this study are included in this article and its supplementary information (SI). Supplementary information is available. See DOI: https://doi.org/10.1039/d5tb00385g.

Acknowledgements

This work was supported by Grants-in-Aid for Japan Agency for Medical Research and Development (AMED) (Grant No. JP22he0422015), the Japan Science and Technology Agency (JST) through the open innovation platform for industry-academia co-creation (COI-NEXT) Program (Grant No. JPMJPF2202), and AMED under Grant Number 24he0122033j0002. This work was partly supported by the Cooperative Research Project of Research Center for Biomedical Engineering (MEXT) and the Project on Design & Engineering by Joint Inverse Innovation for Materials Architecture (MEXT). TDJ wishes to thank the University of Bath and the Open Research Fund of the School of Chemistry and Chemical Engineering, Henan Normal University (2020ZD01), for support. BK.-H. wishes to thank the University of Bath and Lifecare Chemistry for support. JEG wishes to thank Lifecare Chemistry for support. The authors acknowledge Mr Hiroya Hidaka for his valuable assistance with the numerical simulations.

References

1 J. Kim, A. S. Campbell, B. E. F. de Ávila and J. Wang, Wearable biosensors for healthcare monitoring, *Nat. Biotechnol.*, 2019, **37**, 389–406, DOI: 10.1038/s41587-019-0045-y.
2 A. Haleem, M. Javaid, R. P. Singh, R. Suman and S. Rab, Telemedicine for healthcare: capabilities, features, barriers, and applications, *Sens. Int.*, 2021, **2**, 100117, DOI: 10.1016/j.sintl.2021.100117.
3 M. Heckele and W. K. Schomburg, Review on micro molding of thermoplastic polymers, *J. Micromech. Microeng.*, 2004, **14**, R1, DOI: 10.1088/0960-1317/14/3/R01.
4 M. Wang, L. Hu and C. Xu, Recent advances in the design of polymeric microneedles for transdermal drug delivery and biosensing, *Lab Chip*, 2017, **17**, 1373–1387, DOI: 10.1039/C7LC00016B.
5 S. Lin, H. Lin, M. Yang, M. Ge, Y. Chen and Y. Zhu, A two-dimensional MXene potentiates a therapeutic microneedle patch for photonic implantable medicine in the second NIR biowindow, *Nanoscale*, 2020, **12**, 10265–10276, DOI: 10.1039/D0NR01444C.
6 S. F. Lahiji, M. Dangol and H. Jung, A patchless dissolving microneedle delivery system enabling rapid and efficient transdermal drug delivery, *Sci. Rep.*, 2015, **5**, 7914, DOI: 10.1038/srep07914.
7 A. Donadei, H. Kraan, O. Ophorst, O. Flynn, C. O'Mahony, P. C. Soema and A. C. Moore, Skin delivery of trivalent Sabin inactivated poliovirus vaccine using dissolvable microneedle patches induces neutralizing antibodies, *J. Controlled Release*, 2019, **311–312**, 96–103, DOI: 10.1016/j.jconrel.2019.08.039.
8 C. J. Ke, Y. J. Lin, Y. C. Hu, W. L. Chiang, K. J. Chen, W. C. Yang, H. L. Liu, C. C. Fu and H. W. Sung, Multidrug release based on microneedle arrays filled with pH-responsive PLGA hollow microspheres, *Biomaterials*, 2012, **33**, 5156–5165, DOI: 10.1016/j.biomaterials.2012.03.056.
9 L. K. Vora, A. J. Courtenay, I. A. Tekko, E. Larrañeta and R. F. Donnelly, Pullulan-based dissolving microneedle arrays for enhanced transdermal delivery of small and large biomolecules, *Int. J. Biol. Macromol.*, 2020, **146**, 290–298, DOI: 10.1016/j.ijbiomac.2019.12.184.
10 X. Zhang, G. Chen, X. Fu, Y. Wang and Y. Zhao, Magneto-Responsive Microneedle Robots for Intestinal Macromolecule Delivery, *Adv. Mater.*, 2021, **33**, 2104932, DOI: 10.1002/adma.202104932.
11 X. Zhou, B. Li, M. Guo, W. Peng, D. Wang, Q. Guo, S. Wang, D. Ming and B. Zheng, Microneedle patch based on molecular motor as a spatio-temporal controllable dosing strategy of L-DOPA for Parkinson's disease, *Chem. Eng. J.*, 2022, **427**, 131555, DOI: 10.1016/j.cej.2021.131555.
12 J. W. Lee, J. H. Park and M. R. Prausnitz, Dissolving microneedles for transdermal drug delivery, *Biomaterials*, 2008, **29**, 2113–2124, DOI: 10.1016/j.biomaterials.2007.12.048.
13 S. V. Puttaswamy, G. V. Lubarsky, C. Kelsey, X. Zhang, D. Finlay, J. A. McLaughlin and N. Bhalla, Nanophotonic-carbohydrate lab-on-a-microneedle for rapid detection of human cystatin C in finger-prick blood, *ACS Nano*, 2020, **14**, 11939–11949, DOI: 10.1021/acsnano.0c05074.
14 Z. Wang, J. Luan, A. Seth, L. Liu, M. You, P. Gupta, P. Rathi, Y. Wang, S. Cao, Q. Jiang, X. Zhang, R. Gupta, Q. Zhou, J. J. Morrissey, E. L. Scheller, J. S. Rudra and S. Singamaneni, Microneedle patch for the ultrasensitive quantification of protein biomarkers in interstitial fluid, *Nat. Biomed. Eng.*, 2021, **5**, 64–76, DOI: 10.1038/s41551-020-00672-y.
15 A. Mandal, A. V. Boopathy, L. K. W. Lam, K. D. Moynihan, M. E. Welch, N. R. Bennett, M. E. Turvey, N. Thai, J. H. Van, J. C. Love, P. T. Hammond and D. J. Irvine, Cell and fluid sampling microneedle patches for monitoring skin-resident immunity, *Sci. Transl. Med.*, 2018, **10**, eaar2227, DOI: 10.1126/scitranslmed.aar2227.
16 Y. Zheng, R. Omar, R. Zhang, N. Tang, M. Khatib, Q. Xu, Y. Milyutin, W. Saliba, Y. Y. Broza, W. Wu, M. Yuan and H. Haick, A Wearable Microneedle-Based Extended Gate Transistor for Real-Time Detection of Sodium in Interstitial Fluids, *Adv. Mater.*, 2022, **34**, 2270079, DOI: 10.1002/adma.202270079.
17 H. Teymourian, C. Moonla, F. Tehrani, E. Vargas, R. Aghavali, A. Barfidokht, T. Tangkuaram, P. P. Mercier, E. Dassau and J. Wang, Microneedle-Based Detection of Ketone Bodies along with Glucose and Lactate: Toward Real-Time Continuous Interstitial Fluid Monitoring of Diabetic Ketosis and Ketoacidosis, *Anal. Chem.*, 2020, **92**, 2291–2300, DOI: 10.1021/acs.analchem.9b05109.
18 M. J. Fokkert, P. R. van Dijk, M. A. Edens, S. Abbes, D. de Jong, R. J. Slingerland and H. J. Bilo, Performance of the

FreeStyle Libre Flash glucose monitoring system in patients with type 1 and 2 diabetes mellitus, *BMJ Open Diabetes Res. Care*, 2017, **5**, e000320, DOI: **10.1136/bmjdrc-2016-000320**.

19 A. W. Czarnik and T. D. James, Fluorescent chemosensors in the creation of a commercially available continuous glucose monitor, *ACS Sens.*, 2024, **9**, 6320–6326, DOI: **10.1021/acssensors.4c02403**.

20 S. K. Garg, M. Kipnes, K. Castorino, T. S. Bailey, H. K. Akturk, J. B. Welsh, M. P. Christiansen, A. K. Balo, S. A. Brown, J. L. Reid and S. E. Beck, Accuracy and safety of Dexcom G7 continuous glucose monitoring in adults with diabetes, *Diabetes Technol. Ther.*, 2022, **24**, 373–380, DOI: **10.1089/dia.2022.0011**.

21 M. Friedel, I. A. P. Thompson, G. Kasting, R. Polsky, D. Cunningham, H. T. Soh and J. Heikenfeld, Opportunities and challenges in the diagnostic utility of dermal interstitial fluid, *Nat. Biomed. Eng.*, 2023, **7**, 1541–1555, DOI: **10.1038/s41551-022-00998-9**.

22 Y. Kanda, H. Takehara and T. Ichiki, Mechanical strength evaluation of crystalline poly(L-lactic acid) fabricated by replica micromolding for bioabsorbable microneedle devices, *Jpn. J. Appl. Phys.*, 2019, **58**, SDDK05, DOI: **10.7567/1347-4065/ab0ff6**.

23 Y. Kanda, H. Takehara and T. Ichiki, Experimental and numerical studies of deformation of truncated-cone-shaped poly(L-lactic acid) microneedle during insertion, *Appl. Phys. Express*, 2022, **15**, 106503, DOI: **10.35848/1882-0786/ac9453**.

24 M. Fukuhara, H. Takehara, Y. Kanda, A. Matsumoto and T. Ichiki, Functionalization of Poly-L-Lactic Acid Microneedle Tips using Hydrogel Photopolymerization, *J. Photopolym. Sci. Technol.*, 2024, **37**, 233–237, DOI: **10.2494/photopolymer.37.233**.

25 L. Xiao, B. Wang, G. Yang and M. Gauthier, Biomedical Science, *Biomedical Science, Engineering and Technology*, InTech, London, 2012, p. 247, DOI: **10.5772/1020**.

26 A. Södergård and M. Stolt, Properties of lactic acid based polymers and their correlation with composition, *Prog. Polym. Sci.*, 2002, **27**, 1123–1163, DOI: **10.1016/S0079-6700(02)00012-6**.

27 S. Farah, D. G. Anderson and R. Langer, Physical and mechanical properties of PLA, and their functions in widespread applications—A comprehensive review, *Adv. Drug Delivery Rev.*, 2016, **107**, 367–392, DOI: **10.1016/j.addr.2016.06.012**.

28 S. Xu, A. C. Sedgwick, S. A. Elfeky, W. Chen, A. S. Jones, G. T. Williams, A. T. A. Jenkins, S. D. Bull, J. S. Fossey and T. D. James, A boronic acid-based fluorescent hydrogel for monosaccharide detection, *Front. Chem. Sci. Eng.*, 2020, **14**, 112–116, DOI: **10.1007/s11705-019-1812-5**.

29 A. M. Harris and E. C. Lee, Improving mechanical performance of injection molded PLA by controlling crystallinity, *J. Appl. Polym. Sci.*, 2008, **107**, 2246–2255, DOI: **10.1002/app.27261**.

30 H. Tsuji, K. Ikarashi and N. Fukuda, Poly(l-lactide): XII. Formation, growth, and morphology of crystalline residues as extended-chain crystallites through hydrolysis of poly(l-lactide) films in phosphate-buffered solution, *Polym. Degrad. Stab.*, 2004, **84**, 515–523, DOI: **10.1016/j.polymdegradstab.2004.01.010**.

31 D. Battegazzore, S. Bocchini and A. Frache, Crystallization kinetics of poly(lactic acid)-talc composites, *eXPRESS Polym. Lett.*, 2011, **5**, 849–858, DOI: **10.3144/expresspolymlett.2011.84**.

32 I. H. Hillier, Modified avrami equation for the bulk crystallization kinetics of spherulitic polymers, *J. Polym. Sci., Part A*, 1965, **3**, 3067–3078, DOI: **10.1002/pol.1965.100030902**.

33 N. X. Sun, X. D. Liu and K. Lu, An explanation to the anomalous Avrami exponent, *Scr. Mater.*, 1996, **34**, 1201–1207, DOI: **10.1016/1359-6462(95)00657-5**.

34 *In Vitro* Diagnostic Test Systems—Requirements for Blood-Glucose Monitoring Systems for Self-Testing in Managing Diabetes Mellitus, ISO 15197:2013.